ELSEVIER

Biochimica et Biophysica Acta 1460 (2000) 119–132

BIOCHIMICA ET BIOPHYSICA ACTA
BBA

www.elsevier.com/locate/bba

Review

# Lipidic cubic phase crystallization of bacteriorhodopsin and cryotrapping of intermediates: towards resolving a revolving photocycle

Eva Pebay-Peyroula [a], Richard Neutze [b], Ehud M. Landau [c,*]

[a] *Institut de Biologie Structurale, CEA-CNRS-Université Joseph Fourier, 41 rue Jules Horowitz, F-38027 Grenoble Cedex 1, France*
[b] *Department of Biochemistry, Uppsala University, Biomedical Centre, Box 576, S-751 23 Uppsala, Sweden*
[c] *Biozentrum, University of Basel, Klingelbergstrasse 70, 4056 Basel, Switzerland*

Received 24 March 2000; accepted 24 March 2000

**Abstract**

Bacteriorhodopsin is a small retinal protein found in the membrane of the halophilic bacterium *Halobacterium salinarum*, whose function is to pump protons across the cell membrane against an electrostatic potential, thus converting light into a proton-motive potential needed for the synthesis of ATP. Because of its relative simplicity, exceptional stability and the fundamental importance of vectorial proton pumping, bacteriorhodopsin has become one of the most important model systems in the field of bioenergetics. Recently, a novel methodology to obtain well-diffracting crystals of membrane proteins, utilizing membrane-like bicontinuous lipidic cubic phases, has been introduced, providing X-ray structures of bacteriorhodopsin and its photocycle intermediates at ever higher resolution. We describe this methodology, the new insights provided by the higher resolution ground state structures, and review the mechanistic implications of the structural intermediates reported to date. A detailed understanding of the mechanism of vectorial proton transport across the membrane is thus emerging, helping to elucidate a number of fundamental issues in bioenergetics. 

*Keywords:* Bacteriorhodopsin; Crystallization; Photocycle intermediate; Lipidic cubic phase; Membrane protein; X-Ray structure

## 1. Introduction

Nature has provided a great variety of mechanisms for generating a proton-motive gradient across a cell membrane, the centerpiece of Mitchell's theory of chemiosmotic coupling [1] which forms the heart of modern bioenergetics. The inner membrane of mitochondria contains a series of respiratory chain membrane proteins [2] which utilize the energy released by the downhill transfer of electrons from a substrate, NADH or succinate, to a final acceptor, oxygen (which is reduced to water), so as to pump protons. Conversely, the thylakoid membrane of chloroplasts [3] contains a series of membrane protein complexes which harvest energy from visible light so as to drive the uphill transfer of electrons, released through the oxidation of water, to a final electron acceptor ($NADP^+$) and, simultaneously, pump protons. The predominant consumer of the energy stored within a transmembrane proton-motive potential, ATP-synthase, is a highly conserved protein found in mitochondria, chloroplasts, aerobic and photosynthetic

* Corresponding author. Present address: Department of Physiology and Biophysics, University of Texas Medical Branch, 301 University Boulevard, Galveston, TX 77555-0641, USA. Fax: (409) 7723381;
E-mail: emlandau@utmb.edu

0005-2728/00/$ – see front matter 
PII: S0005-2728(00)00134-1

bacteria. The membrane bound component of ATP-synthase ($F_0$-ATPase) couples the back diffusion of protons so as to generate a mechanical torque which is transferred, via the γ-subunit, to the soluble component of ATP-synthase ($F_1$-ATPase) [4] and catalyzes the release of ATP from the $F_1$-ATPase active site. This mechanism maintains the overall displacement of the concentration of ATP (relative to that of ADP and $P_i$) several orders of magnitude from equilibrium, and this excess of ATP acts as the basic energy currency of the cell.

Bacteriorhodopsin (bR) [5] is the simplest known proton pump. It is found in the membrane of *Halobacterium salinarum*, an extremely halophilic bacterium that grows in harsh salt conditions. This small (26 kDa) integral membrane protein contains a chromophore, a retinal molecule covalently bound to Lys216 through a Schiff base linkage, and harvests light energy so as to transport protons from the cytoplasm to the extracellular side of the membrane. The proton-motive potential thereby created couples directly to ATP synthesis. Because of its relative simplicity, exceptional stability and the fundamental importance of vectorial proton pumping, bR has become one of the most important model systems in the field of bioenergetics. Furthermore, its propensity to naturally form two-dimensional crystals in the purple membrane (PM) resulted in it being the first integral membrane protein whose structure has been elucidated. Pioneering two-dimensional electron crystallography studies [6] showed that the protein consists of seven transmembrane α-helices that pack as a trimer within the purple membrane. Further structural characterization [7] suggested the pathway along which protons are transported by the sequence specific exchange of a proton between charged residues.

Bacteriorhodopsin has been a target for X-ray crystallographers in the last 25 years, but resisted almost all attempts, using conventional detergent-based crystallization, to yield well-ordered crystals that diffract to high resolution, with one noteworthy exception [8]. It was only following the recent introduction of a novel crystallization concept using lipidic cubic phases [9] that a dramatic improvement in the resolution attainable in three-dimensional X-ray diffraction studies of the ground state [10,11] as well as the K [12] and $M_N$ [13] intermediate states of bR could be achieved. Another approach for crystallizing bacteriorhodopsin using vesicle fusion recently yielded three-dimensional crystals [14]. In this review we discuss the unique properties of lipidic cubic phases and highlight the predominant changes in our structural understanding of both the ground state of bR, and the intermediates of its photocycle, since the development of lipidic cubic phase crystallization. In Section 2 we describe some of the problems and shortcomings related to conventional crystallization techniques and the properties that render lipidic cubic phases attractive as crystallization matrices for membrane proteins. Section 3 focuses on the X-ray crystallographic structure of bR in the ground state, including the surrounding lipid molecules and water molecules within the protein, as determined from crystals grown in the lipidic cubic phase. Section 4 describes the most recent developments facilitating the structural characterization of the intermediates of the photocycle through kinetic crystallography. Section 5 concludes with reflections on the quest for an atomic level mechanism for vectorial proton transport by bR, and the likely impact of continued kinetic crystallography studies using crystals grown in the lipidic cubic phase.

## 2. Lipidic cubic phases: an alternative approach to membrane protein crystallization

Modern structural biology has witnessed tremendous advances due to rapid developments in the software and hardware available for solving structures of ever more complex biological macromolecules. But whereas the number of soluble protein structures has surpassed 10 000, and the rate of appearance of new structures is increasing steadily, the major stumbling block in attaining high resolution structures of membrane proteins by X-ray crystallography is the expedient and reproducible growth of well-ordered three-dimensional crystals. The difficulty in crystallizing membrane proteins arises from their surface duality: such proteins possess hydrophilic surfaces, which are exposed to the aqueous medium, as well as very hydrophobic surfaces, which interact with the non-polar chains of lipids. Because crystallization requires as a starting point a homogeneous and monodisperse solution of the protein at a relatively high concentration, conditions must be found such that

both hydrophobic and hydrophilic surfaces of the protein will be stably solubilized. Should this basic condition not be fulfilled, then the protein might rapidly aggregate to amorphous species preventing ordered crystal growth. The first breakthrough took place in the early 1970s, when it has been found that detergents are efficient in solubilizing membrane proteins [15,16]. Introduction of detergents led to substantial advances in the area of membrane protein biochemistry, and indeed as early as in 1980 three independent reports of crystallization of membrane proteins appeared [17–19]. However, these crystals were of low quality, and 5 more years elapsed until the first high resolution structure of a membrane protein – a bacterial photosynthetic reaction center – was accomplished [20]. Structural determination of other membrane proteins progressed comparatively slowly, and was limited to proteins that do not denature easily. To date less than 20 high resolution structures of membrane proteins are available.

The reasons for this state of affairs are not absolutely clear. It seems, however, that detergents are not ideal substitutes for the native membrane lipids, as they undergo rapid exchange between the micelles and solubilized monomers [21]. Moreover, in many cases it is very difficult to form monodisperse protein-detergent mixed micelles, and some detergents are notorious for denaturing membrane proteins. We therefore initiated an exploration into alternative means of solubilization, stabilization and crystallization of membrane proteins using lipid bilayers. The system that we developed consists of lipidic cubic phases, which are the most complex structures formed upon mixing lipids with water. Cubic phases exist in two principally different arrangements: the closed discontinuous micellar array, in which lipid micelles are packed in a cubic lattice surrounded by an aqueous compartment (Fig. 1A) and the bicontinuous cubic phase, which exhibits a three-dimensional, continuous membrane bilayer that separates two aqueous channel systems (Fig. 1B). In both systems, water-soluble solutes, such as salts or soluble proteins, freely diffuse in the aqueous compartment. In contrast, lipophilic or amphiphilic compounds, such as membrane proteins and detergent molecules, partition into the lipidic compartment. In the closed micellar array, the long-range lipid diffusion is restricted to exchanges within micelles, with lipid exchange between micelles exceedingly infrequent [22]. In the case of continuous membrane systems, diffusion of both water-soluble and lipid-soluble substances is possible. We therefore hypothesized that labile membrane proteins could be stabilized upon incorporation into continuous bilayers. Subsequent lateral diffusion could form nucleation sites into which the addition of molecules would be facilitated by diffusion along the three-dimensional curved bilayer. This hypothesis provides the basis for our crystallization concept [9,23,24].

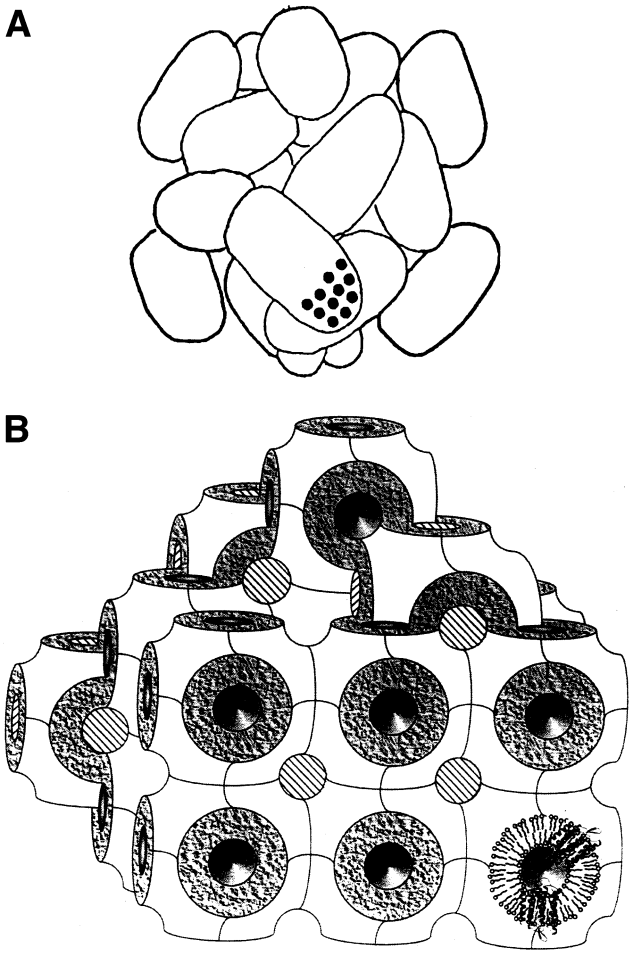


Fig. 1. Schematic representation of the two classes of lipidic cubic phases. (A) The closed discontinuous micellar array, displaying rod-like micelles packed in a cubic lattice and surrounded by an aqueous compartment. (B) The bicontinuous cubic phase, exhibiting a three-dimensional, curved membrane bilayer separating two aqueous channel systems. With permission from CRC Press, Boca Raton, FL.

Crystals of bR obtained in the lipidic cubic phase are typically very small, measuring between 25 and

75 μm in the largest, and 5–10 μm in the smallest dimension. Nonetheless, with the availability of modern synchrotron sources, and especially the microfocus beamline ID13 at the European Synchrotron Radiation Facility (ESRF) in Grenoble, France, we were able to solve the first high resolution structure of bR [25], which was followed by the first complete structure of a biological membrane, the purple membrane, to 1.9 Å resolution [10]. Significantly, bR in such 3D crystals undergoes the well-characterized light-induced photocycle [26], indicating that the structures are biologically relevant. This finding also provided the basis for our subsequent experiments aimed at trapping intermediate states in bR crystals, of which the first high resolution structure of the early intermediate, $K_{LT}$ [12], will be discussed in greater detail in Section 4 of this review. It is noteworthy that lipidic cubic phase crystallization has been successfully used by other groups, solving the high resolution structures of bR in the ground state [11,27] and of the D96N mutant in the ground and $M_N$-intermediate states [13]. Moreover, we have recently demonstrated that bR crystals can be obtained from lipidic cubic phase omitting any use of detergent [28]. Finally, the lipidic cubic phase crystallization approach is not limited to bR, and could be applied to other membrane proteins.

## 3. High resolution structures of bR in the ground state

The first structure of bR, determined by electron crystallography [6,7], revealed a seven-transmembrane helix protein organized as trimers which naturally form 2D crystals in the bacterial membrane, denoted as purple membranes. A seven-transmembrane α-helix motif has since proven to be more general, being shared by other retinal proteins. The initial structure was subsequently improved and refined to 3.5 Å resolution [29]. More recently, electron crystallographic structure to 2.8 Å resolution [30,31] revealed the presence of two β-strands in the BC loop. In parallel, X-ray structures were elucidated from 3D crystals obtained by different approaches: crystals grown from lipidic cubic phases [10,11,25,27], providing the highest resolution, crystals grown from detergent solution by epitaxy [8], and crystals obtained from vesicle fusion [32]. Merohedral twinning was detected in bR crystals grown from lipidic cubic phases [27]. Extensive screening of crystals revealed twinning ratios that vary from 0% to almost 50% and can assume any intermediate value. In the following paragraphs we will first discuss our most recent work on the 1.9 Å resolution ground state structure (Fig. 2) derived from non-twinned crystals [10], and compare it to the results of other groups.

### 3.1. Structure of bR, waters and lipids: the first high resolution structure of a biological membrane

Our high-resolution X-ray structure of bR reveals various interesting aspects: in addition to the precise location of the side chains, a series of well-ordered water molecules within the putative proton pathway, lipid molecules bound to the protein and some aspects of the dynamical properties of the protein have been established. In the 3D crystals grown from lipidic cubic phases bR is arranged as trimers in the ab plane. The trimers have the same hexagonal crystalline arrangement as in the purple patches, and are packed as layers along the c-axis.

The overall structure of bR consists of seven transmembrane α-helices labeled A to G (Fig. 2), linked by loops. The loops are relatively short except loop BC, which forms two antiparallel β-strands on the extracellular surface, and loop EF on the cytoplasmic surface. The C-terminal end of the protein, from residues 233 to 248, is disordered in the crystal and was not located. The chromophore, a retinal, is covalently bound via a Schiff base to Lys216 in helix G. The retinal is buried in a hydrophobic environment located in the core of the protein, formed by several tryptophan residues (W86, W182, W189, W138) which restrict the initial isomerization about the C13 = C14 bond during the photocycle. Extensive studies relating proton transfer measurements and spectroscopic characterization using bR mutants identified the key residues that participate in the proton transfer mechanism. Two residues are of pivotal importance: Asp85 on the extracellular side, and Asp96 on the cytoplasmic side of the Schiff base. Asp85 was identified to be the primary proton acceptor in the early part of the photocycle, whereas Asp96 is the proton donor in the second half of the photocycle.

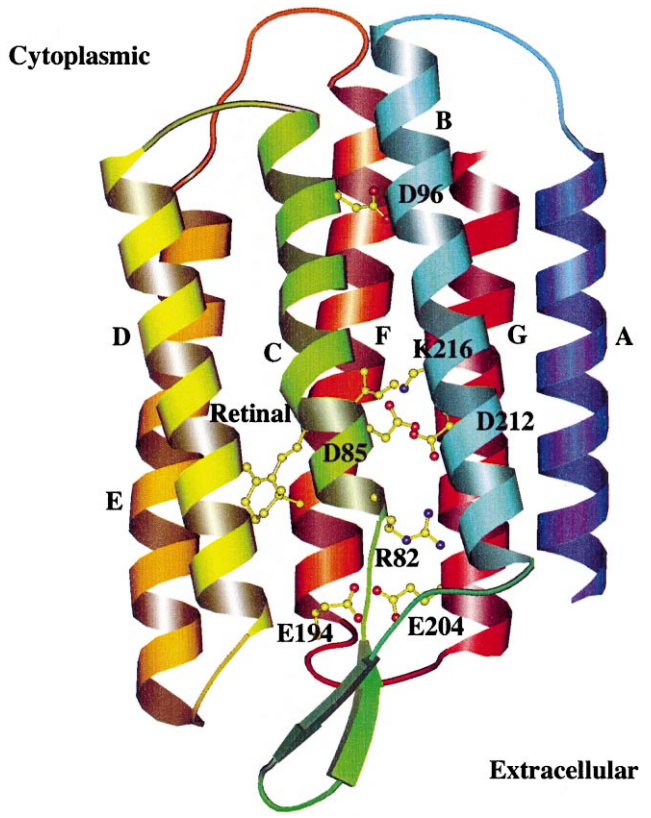


Fig. 2. Overall view of the seven transmembrane helices of bR (entry 1qhj in the protein data bank [10]). The helices are colored according to the sequence numbering: from blue (N-terminus) to red (C-terminus). The residues known to play an important role in the proton translocation, as well as the retinal, are represented.

Eight well-ordered water molecules were located in the extracellular half of the protein within the putative proton transfer pathway (Fig. 3). They form a hydrogen bonded network extending from the Schiff base, which is the primary proton donor located in the middle of the membrane, to Glu194 and Glu204, residues which are known to be involved in the proton release [33] and which are located almost at the EC surface (Figs. 2 and 3). This network includes residues Asp85, the primary proton acceptor, Asp212 and Arg82, all of which are known to be important for proton translocation [34]. The positively charged Schiff base is neighboring to two negatively charged residues, Asp85 and Asp212 on its extracellular side. In the ground state, stabilization of these charged groups is achieved via water molecules, most notably water 402, which bridges between the Schiff base nitrogen and Oδ2 of Asp85. On the cytoplasmic side, no such hydrogen bond network is evident. The entrance into the reprotonation pathway from the cytoplasmic side is in the vicinity of Asp38, and is delineated by several negatively charged residues that form a proton attractive environment: Asp102, Asp104 and Asp36, as well as negatively charged residues of the C-terminal end. The putative proton transfer pathway from Asp96 to the Schiff base is surrounded by hydrophobic residues (Val49, Leu93 and Phe219) and does not show an obvious path for proton transport in the ground state structure, implying the necessity for structural rearrangements facilitating the reprotonation of the Schiff base.

The purple membrane (PM) is a stable and functional entity formed by bR (75% of the total mass) and lipids, which are predominantly polar lipids derived from 2,3-di-*O*-phytanyl-*sn*-glycerol. It was shown that glycolipids are essential in the organization of bR within the PM, presumably by stabilizing

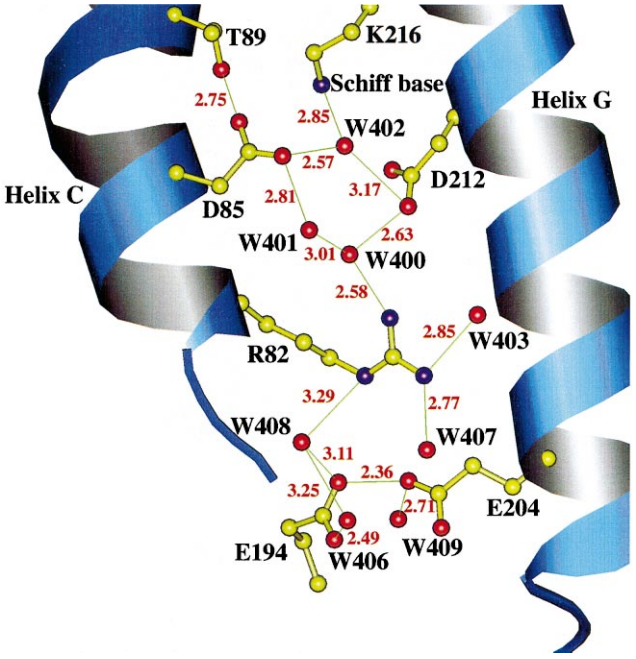


Fig. 3. Hydrogen bonded network in the putative proton translocation pathway from the Schiff base to the extracellular medium. The network connects several of the residues known to be important in the proton transfer, Asp85, Asp212, Arg82, Glu194 and Glu204, as well as water molecules (shown in red). Interatomic distances in Å are shown in red.

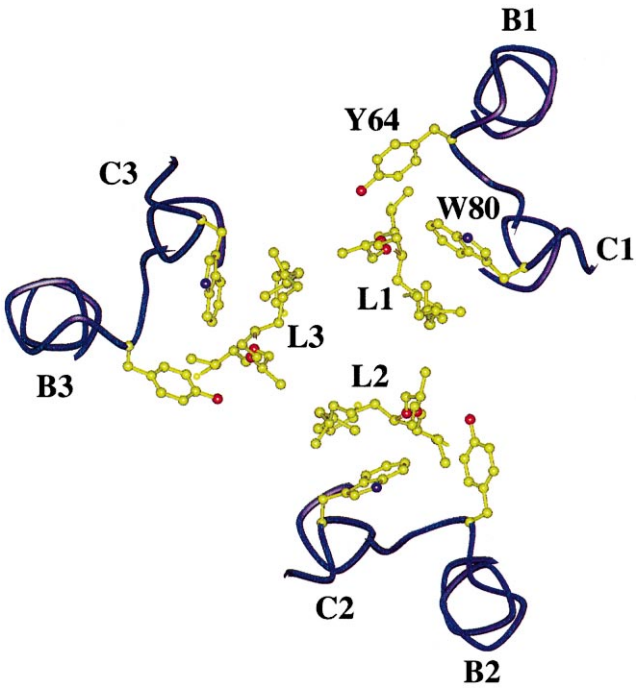


Fig. 4. Lipid/protein interaction. The bR trimer is viewed from the extracellular side toward the interior of the membrane. Lipids L1, L2 and L3, shown in the center of the trimer, are related by a 3-fold symmetry and mediate the trimerization of the protein. The aliphatic chains of the lipids interact with hydrophobic residues in helices B and C of bR (not shown). Tyr64 forms a hydrogen bond with the lipid ether group, and the indole ring of Trp80 interacts with the lipids.

the trimers. Specifically, it was found that PM lipids are important in the formation of the 2D crystals as well as in the kinetics of the photocycle [35]. Packing considerations show that ten lipid molecules can be arranged in the purple membrane per bR monomer. In our electron density maps, nine phytanyl moieties (18 chains) could be located: five in the extracellular and four in the cytoplasmic sides of the protein. In some of the electron densities the aliphatic chains could be clearly identified as phytanyl chains with the characteristic branched methyl groups, but the head groups could not be identified. Mass spectrometric analyses of the crystals and the purple membrane showed that the composition of the lipids in the crystals is the same as that in the PM. Interestingly, bR crystals do not contain any monoolein, which is present in huge excess in the crystallization setups. The head groups of the glycolipids, known to be located on the EC side of the membrane, were located by low resolution neutron diffraction using lipids with deuterated head groups [36]. Their locations are compatible with two phytanyl moieties in our structure: one in the center of the bR trimer (Fig. 4), the second at the periphery of the trimer. Both interact with tryptophan residues, Trp80 and Trp10 or Trp12, respectively.

In addition to providing the atomic positions in a protein structure, X-ray crystallography provides a dynamical parameter, the temperature factor (B-factor). Intrinsically, B-factors are a mixing of static disorder and dynamical properties, and therefore the relative variations of the B-factors within the structure are more relevant than their absolute values. Bacteriorhodopsin exhibits a totally asymmetric B-factor distribution from the extracellular to the cytoplasmic side. In all seven helices the variation follows the same trend: the B-factors are almost constant from the extracellular medium to the center of the membrane, followed by a rapid increase toward the cytoplasm. Marked differences in the stiffness of the protein between the extracellular and the cytoplasmic halves were described earlier [37]. Although not obvious from the ground state structure, this asymmetric distribution certainly has a role in the function of the proton pump. The B-factors follow a similar trend in another high resolution structure of bR grown in the lipidic cubic phase [11].

### 3.2. Comparison with other structures

Various coordinate files of the ground state structure of bR are available in the PDB. An extensive

Table 1
The root-mean-square deviation (r.m.s.d.) between various bR models and our 1qhj model [10]

| Model | 1cw3 [11] | 1brr [8] | 2brd [29] | 2at9 [31] |
|---|---|---|---|---|
| R.m.s.d. on all atoms (Å) | 0.66 | 0.83 | Not determined | Not determined |
| R.m.s.d. on main chain atoms (Å) | 0.45 | 0.52 | 2.03[a] | 1.36[b] |

[a]The largest deviations are located in loops AB, BC and EF.
[b]The largest deviations are located in loops AB and EF.

comparison of some of these structures was recently published [38]. This analysis clearly demonstrated that the overall backbone structures of all are practically the same in the helical regions, as seen in Table 1. Here, we focus on the comparison of the two structures displaying the highest resolution: 1qhj [10] and 1c3w [11]. Both structures were independently obtained from crystals grown in monoolein-based lipidic cubic phases and were solved to 1.9 Å and 1.55 Å resolution, but refined in different ways. The structure by Luecke et al. [11] was solved from data collected from crystals exhibiting 28% twinning. It was refined directly against the experimental intensities using the program ShellX, which is a well-known procedure for dealing with twinning, first developed for small molecule crystals. Our structure to 1.9 Å resolution [10] was solved from non-twinned data and refined in a standard way with the program CNS, commonly used in protein crystallography. Despite the different approaches, the two structures are very similar, exhibiting a root-mean-square deviation (r.m.s.d.) of 0.66 Å and 0.45 Å on all atomic positions, and on the main chain atoms, respectively. The largest deviations are located in loops AB and EF. Twenty-six and 23 water molecules were located in 1qhj and 1c3w respectively, of which 14 are identical, one is displaced by 1.7 Å and the remaining are different. Most of the differences are found among the water molecules situated on the surface of the protein, which might be a consequence of either slightly different crystallization conditions or different refinements. The most interesting water molecules are those located within the putative proton translocation pathway. On the extracellular half of the protein, from the Schiff base to Arg82, the waters are identical in both structures. Deviations appear in the region between Arg82 to Glu194 and Glu204, the proton release dyad (one molecule displaced by 1.7 Å and one additional in 1qhj). The major difference concerns a water molecule which in 1c3w is hydrogen bonded to the carbonyls of Lys216 and Thr46, but is not detected in 1qhj. The lipid chains are globally similar although the connections relating two chains together are different in some of the lipids.

Another recent structure of bR (1brr), refined to 2.9 Å by Essen et al. [8], resulted from crystals grown by a completely different approach: the protein was crystallized by epitaxial growth on benzamidine crystals. As a consequence, the packing is different from that observed in crystals grown from cubic phases. Interestingly bR still packs as a trimer, although not related by a crystallographic symmetry axis. However, in this crystal form the trimers are packed in a head-to-tail arrangement and do not form a purple membrane-like structure. It is noteworthy that two lipid molecules, originating from the purple membrane and co-purified with the protein, could be detected in these crystals: one in the trimer center, which is important for the trimer stability, and the second at the interface between two monomers. Both of these lipids are also present in the previously described structures.

The convergence in the high resolution structures of bR in its ground state provides a solid basis for further structural investigations of the photocycle.

## 4. Structural intermediates in the photocycle of bacteriorhodopsin

### 4.1. Kinetic crystallography

In spite of notable improvements in the resolution of the ground state structures during recent years, a detailed atomic level description of the mechanism of vectorial proton transport by bR is still awaited. A key element in this mechanism is the switching of accessibility from the extracellular to the cytoplasmic side, and in order for it to be understood at the atomic level at least a few of the key photocycle intermediates must be structurally characterized. The tendency of bR to naturally form two-dimensional crystals within the purple membrane has facilitated a number of intermediate trapping and time-resolved studies in two dimensions characterizing the predominant structural rearrangements during the later stages of the photocycle. These studies have been performed using electron diffraction [39–45], neutron diffraction [46–48] and X-ray diffraction [49–54]. Intermediate trapping protocols have been established by controlling the pH, humidity and temperature of the sample, as well as the time delay following a short light pulse prior to flash freezing. Studies have been performed on wild type bR and on a number of mutants. A recent review of this considerable body of work is given by Haupts et al. ([55],

Table 3) and a systematic two-dimensional study of the light induced structural rearrangements during the bR photocycle was recently published [44]. From these accumulated results has emerged the understanding that, during its photocycle, a large scale conformational change occurs in wild type bR approx. 1 ms following illumination, with the strongest changes being observed on helices G, B and F. These conformational changes have been interpreted as an ordering of the cytoplasmic end of helix G and an outward tilt of helix F [40,42,43], which widens the proton channel on the cytoplasmic side and seems likely to play a role in the mechanism of reprotonation of the Schiff base in the second half of the photocycle. Additionally, Bullough and Henderson [56] trapped a low temperature K-intermediate by cooling 2D crystals of wild type bR to 77 K prior to illumination, as did Hendrickson et al. [45] trap a low temperature L-intermediate by cooling glucose embedded 2D crystals of wild type bR to 170 K prior to illumination. Due to limited resolution, neither study revealed any significant change in electron density in projection for these states of the photocycle that occur prior to the deprotonation of the Schiff base.

With the recent availability of high quality three-dimensional crystals grown in the lipidic cubic phase it might be envisioned that pulsed laser triggering, coupled to rapid X-ray diffraction data collection could provide an avenue for structurally characterizing the intermediates of bR's photocycle at high resolution. These methodologies have recently been established via time resolved Laue diffraction studies, with nanosecond resolution, of the photolysis of a carbon monoxide and myoglobin complex [57] as well as the light initiated photocycle of the photoactive yellow protein (PYP) [58]. Practical limitations in the Laue technique [59], primarily the high sensitivity to crystal mosaicity, severely limit the quality of the resulting structural information and appear to rule out any possibility of time resolved studies using a white X-ray beam probe. Fast monochromatic data collection strategies may, superficially, appear to be more feasible when structurally characterizing longer lived structural intermediates. Such an approach, however, requires a large number of oscillation angles to be collected when acquiring a complete data set. With bR crystals grown in lipidic cubic phases the weak crystal contacts between the stacked planes of the purple membrane along the c-axis [25] result in the crystal rapidly becoming highly disordered along that axis after only a small number of turnovers of the photocycle (unpublished results). This rapid disordering precludes the possibility of a complete X-ray diffraction data being recovered from a single crystal at high resolution during a room temperature pump-probe experiment.

Intermediate trapping, or kinetic crystallography, therefore provides the only realistic approach to extract structural information on the intermediates of the bR photocycle. In this approach conditions are found whereby a large population of the desired intermediate builds up within three-dimensional crystals, and monochromatic data collection at low temperatures is used to acquire high quality structural information. The weakness of the technique is that the recovered structural information does not derive from a protein cycling through its photocycle at ambient temperatures. Hence spectroscopic evidence is required to characterize the intermediate trapped at low temperature and to establish its relationship with a physiological intermediate. The power of intermediate trapping techniques, however, lies in the fact that kinetic crystallography provides a direct path to high quality structural information superior to that accessible through a Laue approach, as illustrated by freeze-trapping studies on crystals of the carbon monoxide myoglobin complex [60] and of the photoactive yellow protein [61], which were cooled prior to illumination. To date, structural results from two intermediate trapping protocols have been reported in connection with kinetic crystallography studies on bR using three-dimensional crystals grown in lipidic cubic phases.

### 4.2. *Structural rearrangements during the bacteriorhodopsin photocycle*

An early intermediate in the photocycle was trapped in crystals of wild type bR [12] by first cooling the crystals to 110 K within a cryostream of nitrogen, and subsequently illuminating these crystals with intense green light ($\lambda = 532$ nm). Prior to X-ray diffraction data collection, single crystal microspectrophotometry was used to establish the spectral changes under these conditions, and a spectral shift

to longer wavelength, characteristic of the low temperature K-intermediate ($K_{LT}$) [62] was identified. During X-ray diffraction data collection green light was transported to the crystal via an optical fiber, which rotated with the crystal, thereby maintaining identical conditions to those used during the spectral characterization of the trapped intermediate. X-Ray diffraction data were first screened for merohedral twinning ratios, and only those with twinning ratios less than 2% were selected. Difference electron density maps between the photoexcited and ground state data sets were calculated directly.

A need for caution in developing any trapping protocol can be illustrated by the observation that, at 110 K, the spectral changes strongly depend on the intensity of the illuminating green light. At low intensity the observed population of the $K_{LT}$-intermediate was small, and above a certain threshold intensity the shape of the observed difference spectra changed markedly, presumably due to light induced heating within the core of the protein. As such an optimum between conditions yielding a high population of the desired intermediate, and conditions for which the desired spectral change was visible, was required. This was achieved in practice by recording both X-ray and spectral data over a wide variety of illumination intensities and correlating the observed structural and spectral changes.

The difference electron density map ($F_{exc}-F_{ground}$) for the low temperature K-intermediate, overlaid on the refined ground state model and its $2F_{obs}-F_{calc}$ electron density (light purple), is shown in stereo in Fig. 5a: positive electron density changes are colored blue and negative electron density changes are colored yellow. All negative electron density peaks lie within the ground state electron density, and the positive peaks are displaced by the resolution of the map (2.1 Å) from their corresponding negative feature. A negative electron density peak near the $C_{13}=C_{14}$ isomerized bond (purple) suggests an upward movement of the retinal in this region. This peak, however, is not complemented by an equally strong positive feature, indicating an increased disorder near the isomerized bond. A negative/positive density pair lying on/adjacent to the side chain of Lys216 (cyan), to which the retinal is covalently linked through a protonated Schiff base, represents a sideways movement of this residue caused by the retinal's photoisomerization. The effects of the isomerization also appear to be mechanically transferred along the side chain of Lys216 to its backbone, as a paired negative/positive electron density features on its carbonyl oxygen show a local downward movement at the location of Lys216 along the backbone of helix G very early on in the photocycle. The strongest feature in the difference Fourier map is a negative peak on W402 (red), a water molecule which, in the ground state, separates the negatively charged Asp85 (the primary proton acceptor) and Asp212 [63] from the positively charged Schiff base (the primary proton donor) through the hydrogen bonds illustrated in Fig. 5b. Upon isomerization of the retinal the protonated Schiff base no longer assumes an orientation facilitating the hydrogen bond to this water molecule and, consequently, W402 becomes dislocated. This dislocation of a key water molecule appears to initiate a movement of Asp85 (orange), which shifts towards the position originally occupied by the Schiff base, visualized by the paired negative and positive electron density feature on both the side chain and the carbonyl oxygen of this residue. A smaller positive density feature is also visible near Asp212 (orange), as are weaker positive and negative features seen on Trp86 (white).

The positive and negative electron density changes visible in the difference Fourier map (which displays the least model bias of any crystallographic analysis [64]) were used extensively to interpret the early structural rearrangements in the bR photocycle. These rearrangements were confirmed by refinement, as described in [12], an analysis which also yielded a population of 35% for the trapped intermediate. The refined model (black) is shown in stereo in Fig. 5b and, when overlaid on the ground state model (colored as in Fig. 5a), this structure for $K_{LT}$ displays all the movements described above.

In a second intermediate trapping experiment crystals of the D96N mutant of bR, also grown in the same monoolein-based cubic phase, were used to structurally characterize a later photocycle intermediate [13]. By replacing Asp96, a residue known to play a key role in the reprotonation of the Schiff base during the M to N transition of wild type bR, the lifetime of the late M-state (termed $M_N$-state in the D96N mutant [55]) is considerably prolonged (at pH 7, $\tau$ = tens of seconds). The trapping protocol used

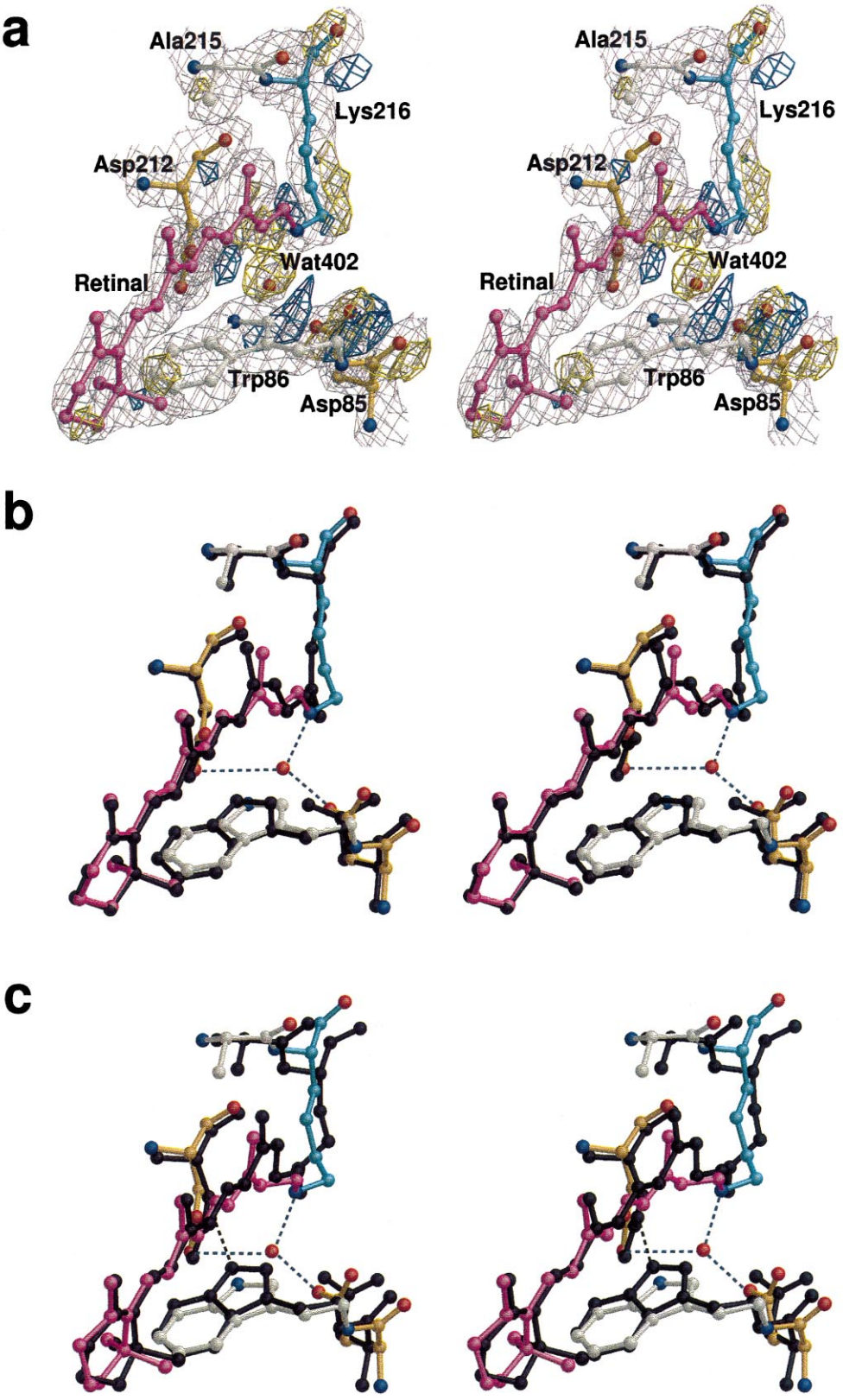
a
Ala215
Lys216
Asp212
Wat402
Retinal
Trp86
Asp85
Ala215
Lys216
Asp212
Wat402
Retinal
Trp86
Asp85
b
c

Fig. 5. Structural changes at the active site of bR during the photocycle. (a) Stereo view of the difference electron density map (yellow, negative; blue, positive density) showing the light induced movements for the low temperature K-intermediate ($K_{LT}$) overlaid on the ground state model and the $2F_{obs}-F_{calc}$ ground state electron density. The retinal (purple), Lys216 (cyan), Asp85 (orange) and Asp212 (orange) are colored. (b) Stereo view of the $K_{LT}$-intermediate (black, entry 1qko of the protein data bank) overlaid on the ground state model (colored as above, the ground state model of 1qkp in the protein data bank). All structural movements visible in the difference electron density map were confirmed by refinement. (c) Stereo view of the $M_N$-intermediate (black) overlaid on the ground state model of the D96N mutant (colored as above, entries 1C8R and 1C8S in the protein data bank). Identical, yet exaggerated, movements are seen at the active site for the $M_N$-intermediate as were seen for the $K_{LT}$-intermediate.
←

was to initially cool crystals to 100 K within a cold nitrogen stream, to then block the nitrogen stream for three seconds while illuminating the crystals with yellow light, and then re-freeze the crystals within the cold nitrogen gas stream [13]. An ambiguity as to the temperature (both the average and the peak) of the crystals during illumination thus arose, and possible implications of this uncertainty on the likely composition of the trapped intermediate state (or states) were not discussed. On the basis of visual inspection of the crystals, which appeared colorless, the trapped intermediate was identified as representing pure M. This was further classified as pure $M_N$ [13] from the knowledge that the lifetime of this sub-state is prolonged in the D96N mutant. Omit electron density maps ($F_{obs}-F_{calc}$) from merohedrally twinned data were used in refitting the retinal, side chain conformations and locating water molecules, and the model was then refined directly using SHELXL-97 (which also refines the merohedral twinning ratio), assuming 100% yield for the trapped intermediate state. Both the refined ground state and excited states models of Luecke et al. are shown in Fig. 5c, viewed from the same angle as that used in Fig. 5a,b.

Despite differences between wild type bR and the D96N mutant used in trapping the $M_N$-intermediate, the very different intermediate trapping protocols, and the subsequent crystallographic analyses used for structurally characterizing the two intermediates, both structures (Fig. 5b,c) show movements of a very similar nature near the active site and there is no doubt that these movements are, in fact, a consequence of the initial light induced retinal isomerization. As would be expected, the movements for the later state are considerably more pronounced than those of the early intermediate, which illustrates that the trapping protocol of Luecke et al. facilitated a greater degree of structural relaxation following photo-excitation than that of Edman et al. For the later intermediate an exaggerated upward movement of the $C_{13}$ methyl group of the retinal ($C_{20}$) pushes against Leu93, which rotates, and Trp182, which moves upwards (neither residue is illustrated), an action which has been anticipated as a mechanism whereby a large movement on the cytoplasmic end of helix F may be induced [43]. Interestingly, the direction of the movement of the primary proton acceptor, Asp85, differs between the two structures: towards the Schiff base for the $K_{LT}$-intermediate and away from the Schiff base for the $M_N$-intermediate. This may reflect the fact that Asp85 and the Schiff base are negatively and positively charged respectively in the early state, and therefore hold a mutual electrostatic attraction, whereas both groups are neutral in the M-state. Along the extracellular proton pumping channel the trapped M-state structure shows that the early dislocation of Wat402 (Fig. 5a) induces further structural disordering which propagates downwards, disrupting the H-bond network formed by the waters Wat400 (Fig. 3, labeled W406 in Luecke et al. [11]) and Wat401, and a new water molecule appears at the center of mass of the positions originally occupied by these waters. Furthermore, the protonated Arg82, which is linked in the ground state structure to Asp85 and Asp212 through this network of water molecules, adopts a downward conformation in the M-state, a mechanism which was suggested to mediate the release of a proton from Glu194 and Glu204 [13], two residues which have been identified as being involved in proton release to the extracellular surface [33].

Despite the prolonged lifetime of the $M_N$-state of the D96N mutant, the large scale structural rearrangements on the cytoplasmic side of the membrane, observed in numerous two-dimensional electron microscopy [40,42–45], X-ray diffraction [49–54] and neutron diffraction [46–48] studies on both wild type bR and the D96N mutant, were not unambig-

uously resolved in three dimensions. The predominant observation by Luecke et al. [13] in this cytoplasmic region was a disordering of the last 12 residues of helix F and the last three residues of helix G. Undoubtedly further M-state structures, from both wild type and mutants using a variety of trapping protocols, will emerge as the debate evolves.

## 5. Conclusions

The considerable improvement in resolution brought about by the lipidic cubic phase crystallization of bR [9] will certainly continue. Two goals concerning these advances would be to recover X-ray diffraction data with sufficient resolution so as to refine the retinal-Schiff base linkage free from geometrical and torsional constraints, and to identify cation binding sites [65–67].

More excitingly, perhaps, is the possibility opened up by the first three-dimensional intermediate structures captured through kinetic crystallography. While the initial structures [12,13] indicate an important mechanistic role for electrostatic interactions, and for the water molecules located in the extracellular half of the proton translocating pathway, a mechanism of vectorial proton transport has not yet emerged in atomic detail. There is, however, no shortage of suggestions. An early proposal that, after the initial retinal isomerization about the $C_{13}=C_{14}$ bond, a second rotation about the $C_{14}$-$C_{15}$ single bond [68] would facilitate the proton transfer to Asp85, appears to be in conflict with later resonance Raman studies [69] indicating that the retinal remains in the 13*cis*-15*anti* configuration throughout the L-, M- and N-intermediates. More recently it has been proposed that a decrease in the curvature of the retinal polyene chain upon deprotonation of the Schiff base, observed in high resolution X-ray diffraction studies of a number of retinylidene compounds, can act as a mechanism for switching the Schiff base access from the extracellular side to the cytoplasmic side following the primary proton transfer event [44]. Luecke et al. [13] argued that the reorientation of Arg82 observed in their $M_N$ structure plays a key role the vectoriality of the proton transfer. Upon proton release this movement was suggested to push the equilibrium towards the late M-state, and the resulting high p$K_a$ of Asp85 ensures that the Schiff base is reprotonated from the cytoplasmic side.

Further characterization of the structural changes during bR's photocycle is required so as to unambiguously establish the mechanism of vectoriality. The underlying principles of vectorial transport thereby revealed will certainly have relevance to the pumping mechanism of the respiratory chain terminal oxidases [70], the coupling of proton back-diffusion to a mechanical rotation by the membrane bound $F_0$-ATPase [71], and on membrane transport in general.

## Acknowledgements

We thank H. Belrhali, K. Edman, J. Hajdu, A. Hardmeyer, C. Menzel, J. Navarro, P. Nollert, J.P. Rosenbusch and A. Royant for discussions, criticism, encouragement and experimental contributions. These studies were supported by grants from the EU-BIOTECH, the Swedish Research Council NFR, the Institut Universitaire de France and the Swiss National Science Foundation's SPP BIOTECH. Continuous allocation of synchrotron beamtime at ESRF is greatly acknowledged.

## References

[1] P. Mitchell, Nature 191 (1961) 144–148.
[2] M. Saraste, Science 283 (1999) 1488–1493.
[3] S. Berry, B. Rumberg, Biochim. Biophys. Acta 1410 (1999) 248–261.
[4] J.P. Abrahams, A.G.W. Leslie, R. Lutter, J.E. Walker, Nature 370 (1994) 621–628.
[5] D. Oesterhelt, W. Stoeckenius, Nat. New Biol. 233 (1971) 149–152.
[6] R. Henderson, P.N.T. Unwin, Nature 257 (1975) 28–32.
[7] R. Henderson, J.M. Baldwin, T.A. Ceska, F. Zemlin, E. Beckmann, K.H. Downing, J. Mol. Biol. 213 (1990) 899–929.
[8] L.-O. Essen, R. Siegert, W.D. Lehmann, D. Oesterhelt, Proc. Natl. Acad. Sci. USA 95 (1998) 11673–11678.
[9] E.M. Landau, J.P. Rosenbuch, Proc. Natl. Acad. Sci. USA 93 (1996) 14532–14535.
[10] H. Belrhali, P. Nollert, A. Royant, C. Menzel, J.P. Rosenbusch, E.M. Landau, E. Pebay-Peyroula, Structure 7 (1999) 909–917.
[11] H. Luecke, B. Schobert, H.T. Richter, J.-P. Cartailler, J.K. Lanyi, J. Mol. Biol. 291 (1999) 899–911.

[12] K. Edman, P. Nollert, A. Royant, H. Belrhali, E. Pebay-Peyroula, J. Hajdu, R. Neutze, E.M. Landau, Nature 401 (1999) 822–826.
[13] H. Luecke, B. Schobert, H.T. Richter, J.-P. Cartailler, J.K. Lanyi, Science 286 (1999) 255–260.
[14] K. Takeda, H. Sato, T. Hino, M. Kono, K. Fukuda, I. Sakurai, T. Okada, T. Kouyama, J. Mol. Biol. 283 (1998) 463–474.
[15] A. Helenius, K. Simons, Biochim. Biophys. Acta 415 (1975) 29–79.
[16] C. Tanford, J.A. Reynolds, Biochim. Biophys. Acta 457 (1976) 133–170.
[17] R.M. Garavito, J.P. Rosenbusch, J. Cell Biol. 86 (1980) 327–329.
[18] R. Henderson, D. Shotton, J. Mol. Biol. 139 (1980) 99–102.
[19] H. Michel, D. Oesterhelt, Proc. Natl. Acad. Sci. USA 77 (1980) 1283–1285.
[20] J. Deisenhofer, O. Epp, K. Miki, R. Huber, H. Michel, Nature 318 (1985) 618–624.
[21] M. Zulauf, J.P. Rosenbusch, J. Phys. Chem. 87 (1983) 856–862.
[22] S. Cribier, A. Gulik, P. Fellmann, R. Vargas, P.F. Devaux, V. Luzzati, J. Mol. Biol. 229 (1993) 517–525.
[23] E.M. Landau, G. Rummel, S.W. Cowan-Jacob, J.P. Rosenbusch, J. Phys. Chem. B 101 (1997) 1935–1937.
[24] G. Rummel, A. Hardmeyer, C. Widmer, M.L. Chiu, P. Nollert, K.P. Locher, I. Pedruzzi, E.M. Landau, J.P. Rosenbusch, J. Struct. Biol. 121 (1998) 82–91.
[25] E. Pebay-Peyroula, G. Rummel, J.P. Rosenbusch, E.M. Landau, Science 277 (1997) 1676–1681.
[26] J. Heberle, G. Büldt, E. Koglin, J.P. Rosenbusch, E.M. Landau, J. Mol. Biol. 281 (1998) 587–592.
[27] H. Luecke, H.T. Richter, J.K. Lanyi, Science 280 (1998) 1934–1937.
[28] P. Nollert, A. Royant, E. Pebay-Peyroula, E.M. Landau, FEBS Lett. 457 (1999) 205–208.
[29] N. Grigorieff, T.A. Ceska, K.H. Downing, J.M. Baldwin, R. Henderson, J. Mol. Biol. 259 (1996) 393–421.
[30] Y. Kimura, D.G. Vassylyev, A. Miyazawa, A. Kidera, M. Matsushima, K. Mitsuoka, K. Murata, T. Hirai, Y. Fujiyoshi, Nature 389 (1997) 206–211.
[31] K. Mitsuoka, T. Hirai, K. Murata, A. Miyazawa, A. Kidera, Y. Kimura, Y. Fujiyoshi, J. Mol. Biol. 286 (1999) 861–882.
[32] H. Sato, K. Takeda, T. Hino, T. Okada, M. Nakasako, N. Kamiya, T. Kouyama, Acta Crystallogr. D 56 (1999) 1251–1256.
[33] A.K. Dioumaev, H.T. Richter, L.S. Brown, M. Tanio, S. Tuzi, H. Saito, Y. Kimura, R. Needleman, J.K. Lanyi, Biochemistry 37 (1998) 2496–2506.
[34] H.G. Khorana, Proc. Natl. Acad. Sci. USA 90 (1993) 1166–1171.
[35] B. Sternberg, C. L'Hostis, C.A. Whiteway, A. Watts, Biochim. Biophys. Acta 1108 (1992) 21–30.
[36] M. Weik, H. Patzelt, G. Zaccai, D. Oesterhelt, Mol. Cell 1 (1998) 411–419.
[37] V. Réat, H. Patzelt, C. Pfister, M. Ferrand, D. Oesterhelt, G. Zaccai, Proc. Natl. Acad. Sci. USA 95 (1998) 4970–4975.
[38] S. Subramaniam, Curr. Opin. Struct. Biol. 9 (1999) 462–468.
[39] R.M. Glaeser, J. Baldwin, T.A. Ceska, R. Henderson, Biophys. J. 50 (1986) 913–920.
[40] S. Subramaniam, A.R. Faruqi, D. Oesterhelt, R. Henderson, Proc. Natl. Acad. Sci. USA 94 (1997) 1767–1772.
[41] B.G. Han, J. Vonck, R.M. Glaeser, Biophys. J. 67 (1994) 1179–1186.
[42] J. Vonck, Biochemistry 35 (1996) 5870–5878.
[43] S. Subramaniam, M. Gerstein, D. Oesterhelt, R. Henderson, EMBO J. 12 (1993) 1–8.
[44] S. Subramaniam, M. Lindahl, P. Bullough, A.R. Faruqi, J. Tittor, D. Oesterhelt, L. Brown, J. Lanyi, R. Henderson, J. Mol. Biol. 287 (1999) 145–161.
[45] F.M. Hendrikson, F. Burkard, R.M. Glaeser, Biophys. J. 75 (1998) 1446–1454.
[46] N.A. Dencher, D. Dresselhauss, G. Zaccai, G. Bueldt, Proc. Natl. Acad. Sci. USA 86 (1989) 7876–7879.
[47] T. Hauss, G. Bueldt, M.P. Heyn, N.A. Dencher, Proc. Natl. Acad. Sci. USA 91 (1994) 11854–11858.
[48] M. Weik, G. Zaccai, N.A. Dencher, D. Oesterhelt, T. Hauss, J. Mol. Biol. 275 (1998) 625–634.
[49] M. Nakasako, M. Kataoka, Y. Amemiya, F. Tokunaga, FEBS Lett. 292 (1991) 73–75.
[50] M.H.J. Koch, N.A. Dencher, D. Oesterhelt, H.J. Ploehn, G. Rapp, G. Bueldt, EMBO J. 10 (1991) 521–526.
[51] H. Kamikubo, M. Kataoka, G. Varo, T. Oka, F. Tokunaga, R. Needleman, J.K. Lanyi, Proc. Natl. Acad. Sci. USA 93 (1996) 1386–1390.
[52] H. Kamikubo, T. Oka, Y. Imamoto, F. Tokunaga, J.K. Lanyi, M. Kataoka, Biochemistry 36 (1997) 12282–12287.
[53] H.J. Sass, I.W. Schachowa, G. Rapp, M.H.J. Koch, D. Oesterhelt, N.A. Dencher, G. Bueldt, EMBO J. 16 (1997) 1484–1491.
[54] H.J. Sass, R. Gessenich, M.H.J. Koch, D. Oesterhelt, N.A. Dencher, G. Bueldt, G. Rapp, Biophys. J. 75 (1998) 399–405.
[55] U. Haupts, J. Tittor, D. Oesterhelt, Annu. Rev. Biophys. Biomol. Struct. 28 (1999) 367–399.
[56] P.A. Bullough, R. Henderson, J. Mol. Biol. 286 (1999) 1663–1671.
[57] V. Srajer, T.Y. Teng, T. Ursby, C. Pradervand, Z. Ren, S. Adachi, W. Schildkamp, D. Bourgeois, M. Wulff, K. Moffat, Science 274 (1996) 1726–1729.
[58] B. Perman, V. Srajer, Z. Ren, T.Y. Teng, C. Pradervand, T. Ursby, D. Bourgeois, F. Schotte, M. Wulff, R. Kort, K. Hellingwerf, K. Moffat, Science 279 (1998) 1946–1950.
[59] J. Hajdu, I. Andersson, Annu. Rev. Biophys. Biomol. Struct. 22 (1993) 467–498.
[60] I. Schlichting, J. Berendzen, G.N. Phillips Jr., R.M. Sweet, Nature 371 (1994) 808–812.
[61] U.K. Genick, S.M. Soltis, P. Kuhn, I.L. Canestrelli, E.D. Getzoff, Nature 392 (1998) 206–209.
[62] S.J. Doig, P.J. Reid, R.A. Mathies, J. Phys. Chem. 95 (1991) 6372–6379.

[63] M.S. Braiman, T. Mogi, T. Marti, L.J. Stern, H.G. Khorana, K.J. Rothschild, Biochemistry 27 (1988) 8516–8520.
[64] R. Henderson, J.K. Moffatt, Acta Crystallogr. B 27 (1971) 1414.
[65] R.R. Birge, D.S.K. Govender, K.C. Izgi, E.R.L. Tan, J. Phys. Chem. 100 (1996) 9990–10004.
[66] G. Varo, L.S. Brown, R. Needleman, J.K. Lanyi, Biophys. J. 76 (1999) 3219–3226.
[67] S. Tuzi, S. Yamaguchi, M. Tanio, H. Koniski, S. Inove, A. Naito, R. Needleman, J.K. Lanyi, H. Saito, Biophys. J. 76 (1999) 1523–1531.
[68] K. Schulten, P. Tavan, Nature 272 (1978) 85–86.
[69] S.P. Fodor, J.B. Ames, R. Gebhard, E.M. van der Berg, W. Stoeckenius, J. Lugtenburg, R.A. Mathies, Biochemistry 27 (1988) 7097–7101.
[70] S. Iwata, C. Ostermeier, B. Ludwig, H. Michel, Nature 376 (1995) 660–669.
[71] D. Stock, A.G.W. Leslie, J.E. Walker, Science 286 (1999) 1700–1705.